Controlling Optically-Driven Atomic Migration Using Crystal-Facet Control in Plasmonic Nanocavities

Angelos Xomalis [1†*], Rohit Chikkaraddy [1†], Eitan Oksenberg[2], Ilan Shlesinger[2], Junyang Huang [1], Erik C. Garnett[2,3], A. Femius Koenderink[2], Jeremy J. Baumberg [1*]

[1] NanoPhotonics Centre, Cavendish Laboratory, Department of Physics, JJ Thompson Avenue, University of Cambridge, Cambridge, CB3 0HE, United Kingdom

[2]Center for Nanophotonics, AMOLF, Science Park 104, 1098 XG, Amsterdam, The Netherlands

[3]Van der Waals-Zeeman Institute, University of Amsterdam, Science Park 904, 1090 GL, Amsterdam, The Netherlands

ABSTRACT

Plasmonic nanoconstructs are widely exploited to confine light for applications ranging from quantum emitters to medical imaging and biosensing. However, accessing extreme near-field confinement using the surfaces of metallic nanoparticles often induces permanent structural changes from light, even at low intensities. Here, we report a robust and simple technique to exploit crystal facets and their atomic boundaries to prevent the hopping of atoms along and between facet planes. Avoiding X-ray or electron microscopy techniques that perturb these atomic restructurings, we use elastic and inelastic light scattering to resolve the influence of crystal habit. A clear increase in stability is found for {100} facets with steep inter-facet angles, compared to multiple atomic steps and shallow facet curvature on spherical nanoparticles. Avoiding atomic hopping allows Raman scattering on molecules with low Raman cross-section while circumventing effects of charging and adatom binding, even over long measurement times. These nano-constructs allow the optical probing of dynamic reconstruction in nanoscale surface science, photocatalysis, and molecular electronics.

KEYWORDS

nanocavity, nano-optics, SERS, atomic hopping, crystal facet, single-molecule, picocavity

Nanoconstructs of noble metals are providing a plethora of research directions leading to the realisation of single-molecule spectroscopies which conventional top-down fabrication techniques have struggled to reach.[1-3] Metallic nanocavities offer extreme light confinement with atomic-scale resolution[4, 5] that can boost the detection sensitivity of molecular vibrations while their plasmonic response can be spectrally tuned through the structure morphology.[6-8] In this way, large scale, cost-effective and self-assembled techniques can assist studying plasmonic near-field enhancements[9] and contributing to technological breakthroughs ranging from nano-heat reservoirs[10] and pyroelectric photodetectors,[11] to photovoltaics[12] and plasmon-mediated photocatalysis.[13]

The enhanced near-fields arising from free-electron collective oscillations in plasmonic media are strongly dependent on the shape of their nanostructures. Million-fold optical intensity enhancements are achieved in sub-nm gaps formed between two noble metal nanostructures.[14] In such scenarios

contributions from atomic-scale morphology play an important role in controlling the near-field. Atomic structures such as crystallographic planes, facets, and atomic steps within nanogaps directly influence the resulting near-field 'hot-spot' distribution.[4] Consequently, considerable effort has been devoted to controlling the growth of nanocrystals, deciphering their influence on plasmonic properties of NPs and estimating the surface energy of primary and high index facets.[15-18]

RESULTS AND DISCUSSION

Here, we experimentally study the atomic movement of Au atoms on {111} and {100} facets in nanogaps. Nanospheres (NP) and nanocubes (NC) with different crystal facets are assembled on atomically flat mirrors coated with closely-packed self-assembled molecular layers, resulting in a nanostructure-on-mirror geometry (respectively NPoM and NCoM, Fig. 1a,d). The NPoMs have {111} gap facets produced when the triangular facets align face-down on the mirror (Fig. 1b), while NCoMs have {100} facets sitting on the gap formed between nanoparticle and mirror (Fig. 1e).[19] By using dark-field scattering and surface-enhanced Raman scattering (SERS) we detect individual Au atom hopping events inside self-assembled nanogaps. We find that single-crystal plasmonic nanoconstructs based on the NCoM geometry give much larger power thresholds for atom migration compared to more globular NPoM structures. Due to their high stability such nanoconstructs enable SERS measurements on molecules with low Raman cross-sections which demand higher pump powers.

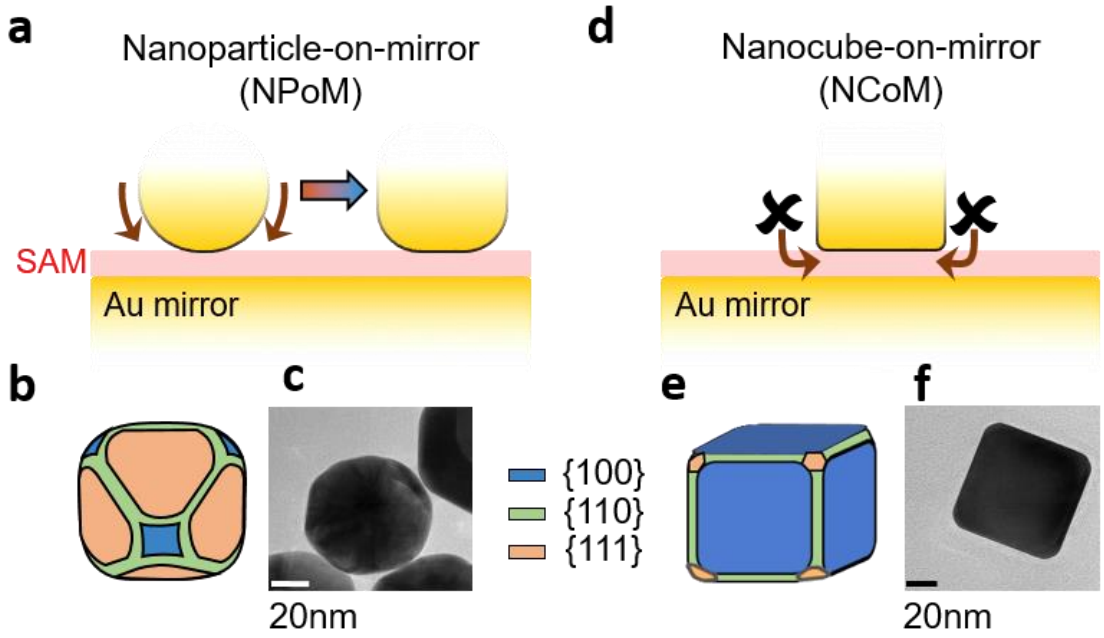

Fig. 1: Atomic hopping and nanoparticle reconstruction. a) Schematic of NPoM system illustrating atom hopping gradually growing the facet width under intense light illumination. **b)** Primary crystallographic facets of globular nanoparticles. **c)** TEM of 80 nm diameter NP. **d)** Schematic showing NCoM sustains its shape under illumination due to large energy barriers at edges. **e,f)** As (b,c) for 75 nm NCoM. Molecular layer is biphenyl-4-thiol (BPT) that creates nanogaps of 1.3 ± 0.1 nm.[20]

The growth and shape control of nanocrystals is an ongoing challenge in materials science with Au being one of the few materials where a high degree of shape control has been demonstrated.[21] Both the nanocube and nanosphere AuNPs are citrate capped which, compared to PVP-ligand coatings, allows much smaller nanoparticle gaps to form thus, giving much higher optical confinement.[22] The Au mirror substrates are prepared by e-beam deposition on Si wafers using a template-stripping method.[23] For the formation of self-assembled monolayers, the substrates are immersed for 12h in 1mM biphenyl-4-thiol (BPT) in anhydrous ethanol (see Methods).[24] Au NPs are then deposited onto the SAM-coated Au substrates by drop-casting.

Dark-field images of such plasmonic nanostructures spaced above flat Au by ultrathin molecular spacers reveal a rich collection of colours resulting from the various scattering resonances, which we record using confocal spectroscopy (see Methods). The optics of such cubic nanoconstructs have been thoroughly characterised previously.[25-37] Based on a spherical harmonics description, the two dominating modes for such small gaps are labelled (10) and (20)[22, 38] and are accessed from large angle excitation using high NA optics.[39] We emphasise that these modes are different from the $(11)_{x,y}$ modes typically accessed at normal incidence in NCoMs with larger gaps (>5 nm),[34] which for the small gaps here red-tune beyond 1 µm wavelengths and possess negligible optical coupling efficiency.[22]

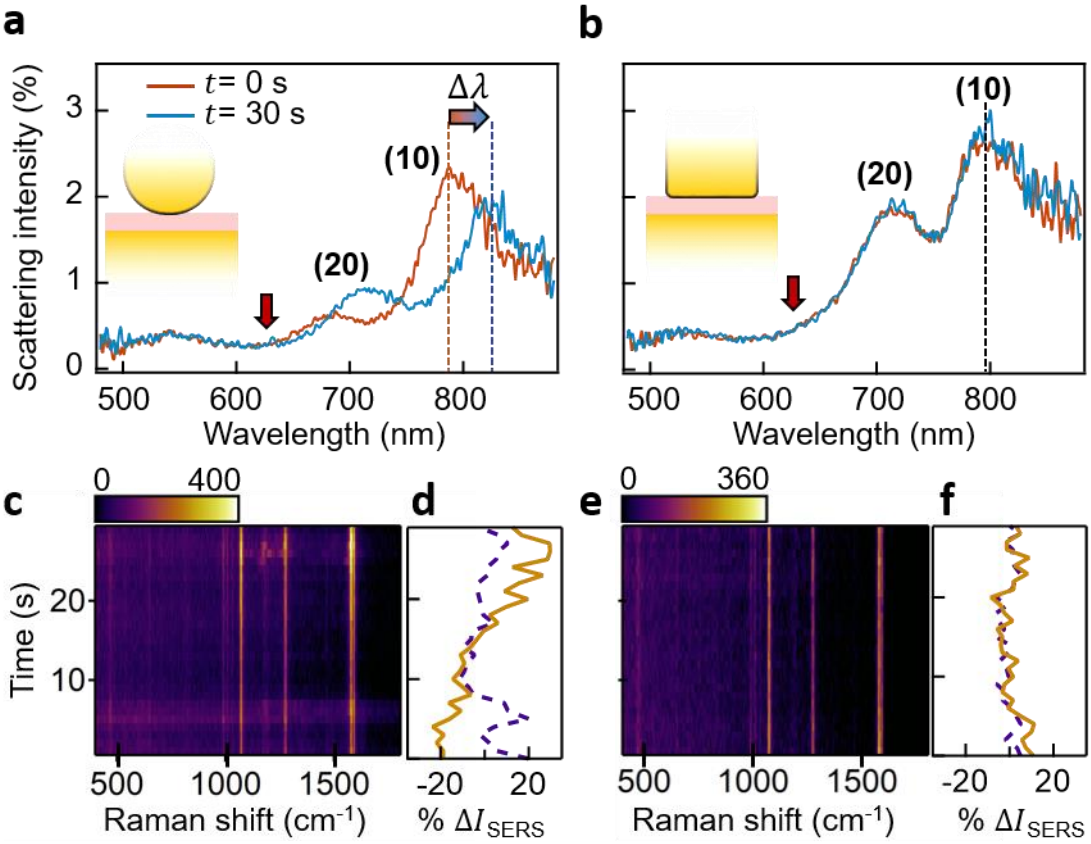

Fig. 2: Nanostructure resilience to laser illumination. a,b) Scattering spectra of (a) NPoM and (b) NCoM, measured before (orange) and after 30 s (blue) of continuous laser illumination. **c)** SERS time scans for NPoM, showing unstable backgrounds and appearance of new vibrational lines. **d)** Variation in SERS intensity of 1580 cm^{-1} vibrational mode (orange) and background (purple dashed). **e,f)** As (c,d) for NCoM, showing no new vibrational lines or changes in the background. Pump laser is 633 nm (red arrows in a,b) with intensity 200 µW/µm^2 in all cases.

The nanocavity modes for d=1.3 nm gaps are exceptionally sensitive to variations of the NP facets and gap geometry, and in particular redshifts of the (10) mode track increases in the facet size.[40, 41] Here, extreme light confinement produces up to 100-fold compressed plasmonic wavelengths, which can resolve atomic reconstruction of 3D objects. Detailed full-wave simulations, analytic models and experiments show that 1% redshift in the (10) mode ($\Delta\lambda$ = 8 nm) corresponds to the arrival of only ~500 atoms onto the facet, or a change in facet radius of less than 1 atom.[38, 40, 42] This allows real-time dark-field measurements to detect nanoscale reconstruction by comparing between NPoMs and NCoMs before (orange line) and after 30 s (blue line) of continuous laser illumination (Fig. 2a,b). These show similar scattering strength at the 633 nm pump wavelength (red arrows). However, while the NPoM (10) mode resonance redshifts by ~40 nm, the spectral peak for the NCoM remains stable at

800 nm. The pump wavelength is chosen in order to amplify the Stokes region of the SERS through the plasmon resonance of the nanoconstructs.[43]

To investigate the NP stability in more detail, SERS spectra are recorded sequentially in time (every 1s) observing the vibrational resonances of the self-assembled monolayer of BPT used as the dielectric spacer (Fig. 2c,e). Previous work has shown that large variations of SERS intensity indicate changes in local field enhancement E since $I_{SERS} \propto [E(\lambda_{\mathrm{in}})]^2[E(\lambda_{\mathrm{out}})]^2$. The similar dark-field scattering amplitudes indicate similar coupling efficiencies for these NCoMs and NPoMs, and indeed the SERS intensities are thus also similar.

Despite this, the stability of the SERS shows great differences. Extracting the fractional changes in SERS intensity for the strongest vibrational mode at 1580 cm^{-1} (orange line) and the background (purple dashed line) (Fig. 2d,f) shows a root-mean-square variation in NPoMs which is >3 times larger than in NCoMs (where this residual mostly arises from small mechanical movements of the sample under the laser spot). We note that background variations are also higher in NPoMs, and may be correlated to local reductions of the plasma frequency. This allows more field to penetrate into the metal which increases the electronic Raman scattering (making up the SERS background).[44, 45] The NPoM constructs all show changes in SERS intensity >40%, associated with the progressive detuning of the plasmon resonance as the facet diameter increases.[46] In addition, transient vibrational lines are also observed, arising from the mobilisation of adatoms in the gap which fleetingly result in extreme near-field hot-spots (<1 nm^3).[14] No such transients are observed in the case of NCoM plasmonic constructs.

To better quantify these fluctuations we perform systematic studies on 20 particles. Extracting the spectral position of plasmon resonances before (red) and after (blue) laser illumination for NPoM and NCoM nanoconstructs shows the much larger shifts for NPoMs (Fig. 3a,b, bold line in box gives mean value, and its outline gives 85% deviation from mean). The spectral distribution of the NPoMs increases as well as shifts to longer wavelength, which directly indicates their increasing facet size and changing shape (Fig. 3a). The plasmon resonance for NCoMs instead remains at 780 nm (Fig. 3c). In addition, histograms showing the percentage variation in SERS intensity after 30 s (Fig. 3b,d) reveal that it is five-fold larger in NPoMs (∼25%) compared to NCoMs (<5%) for constant power density. In all cases, the laser optical intensity is 200 $\mu W/\mu m^2$ at an excitation wavelength of 633 nm.

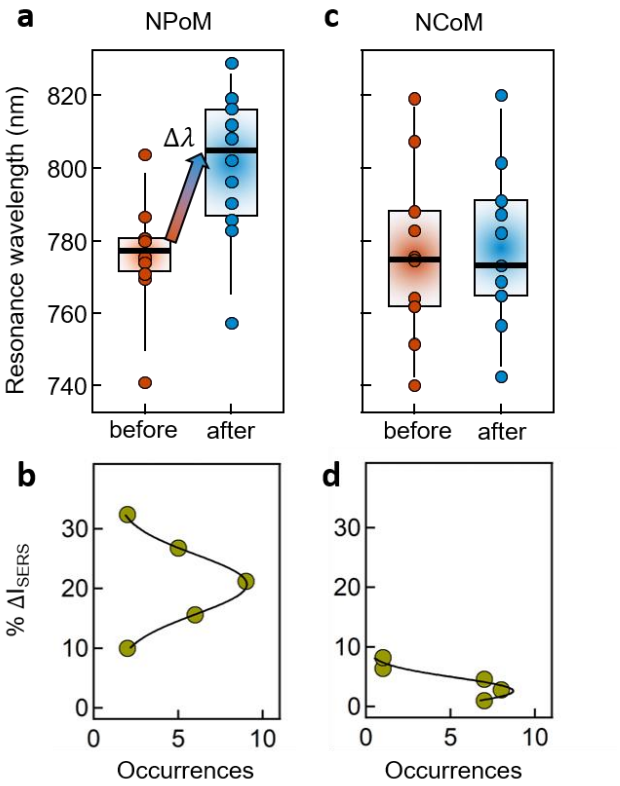

Fig. 3: Nanoparticles shape reconstruction seen *via* dark-field scattering and SERS. a,c) Shift in spectral position (Δλ) of plasmon resonances recorded before (red) and after (blue) 30 s of continuous laser illumination. Outline of box indicates 85% deviation from mean value (bold horizontal line). **b,d)** Variation of SERS intensity for NPoM and NCoM nanocavities, fit to Gaussian distribution. Irradiation intensity is 200 μW/μm^2.

These fluctuations are driven by light, as revealed by power-dependent measurements while increasing the optical intensity from I = 0.2 to 2.0 mW/μm^2. At these intensities the NPoM systems are wildly unstable with thresholds always below 0.05 mW/μm^2. By contrast, for NCoM nanoconstructs at low power the plasmonic resonances remain stable, and they redshift slightly only at much higher irradiation intensities (Fig. 4a), with each resonance shifting differently. While the (20) resonance shows little tuning, the long wavelength (10) mode can be redshifted ~15 nm. This is expected for the larger cube facets where more of the mode tuning is transferred onto the longer wavelength (10) mode.[22, 38, 46] For different NCoMs, the power thresholds differ. This is quantified by fitting the power threshold (I_{th}) using a sigmoidal dependence $\lambda = \lambda_o + K[1 + \exp\{-(I - I_{\mathrm{th}})/R\}]^{-1}$ (Fig. 4b,c). Across many NCoMs these fits show that the longer wavelength (10) average mode threshold $\bar{I}_{\mathrm{th}}$=0.7 mW/μm^2 is half that of the shorter wavelength (20) mode of 1.4 mW/μm^2 (Fig. 4d).

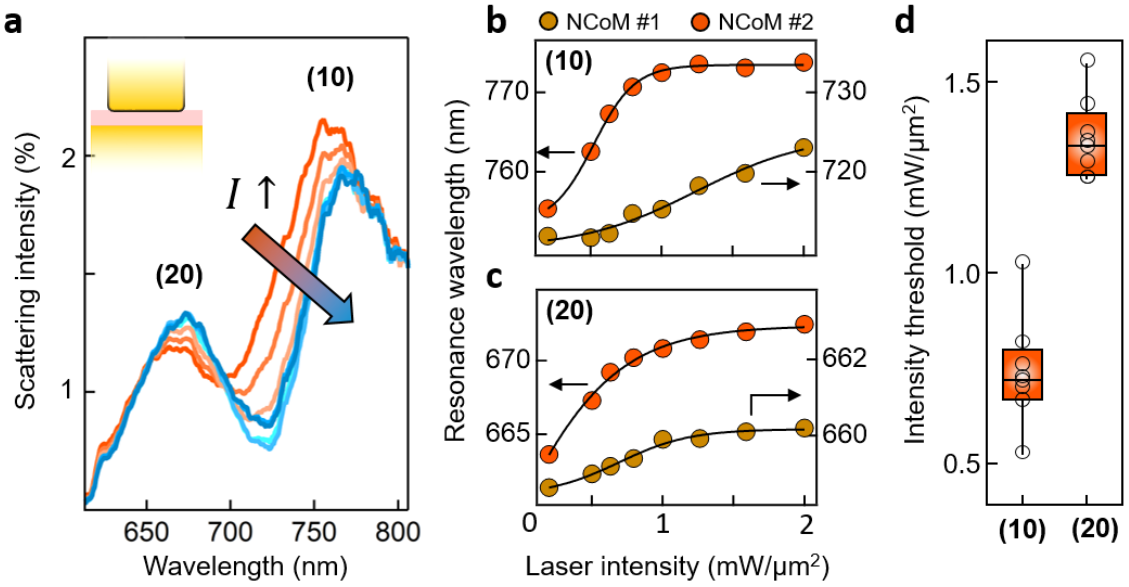

Fig. 4: Plasmon resonance shifts of NCoMs with laser intensity. a) Dark-field scattering spectra with increasing laser intensity. **b,c)** Plasmon resonance shifts of two NCoMs for (10) and (20) modes *vs* laser intensity. **d)** Intensity thresholds extracted from sigmoidal fits (box outlines 85% closest to mean).

To demonstrate the importance of these evident differences in atomic-scale stability, we show how it allows access to a much wider range of molecular targets than previously. These small gap plasmonic cavities have already demonstrated key advantages in providing large enough SERS enhancements so that molecules which have no electronic resonances close to the laser wavelength can be used. Avoiding direct pumping into higher electronic states removes the inevitable bleaching that also plagues fluorescence-based sensing. Molecules without delocalised π-systems typically have low Raman cross-sections and it has thus proved hard to extract signals from fewer than many millions of them. Here we show a simple carboxylate can be sensed at the <100 molecule level for long periods of time.

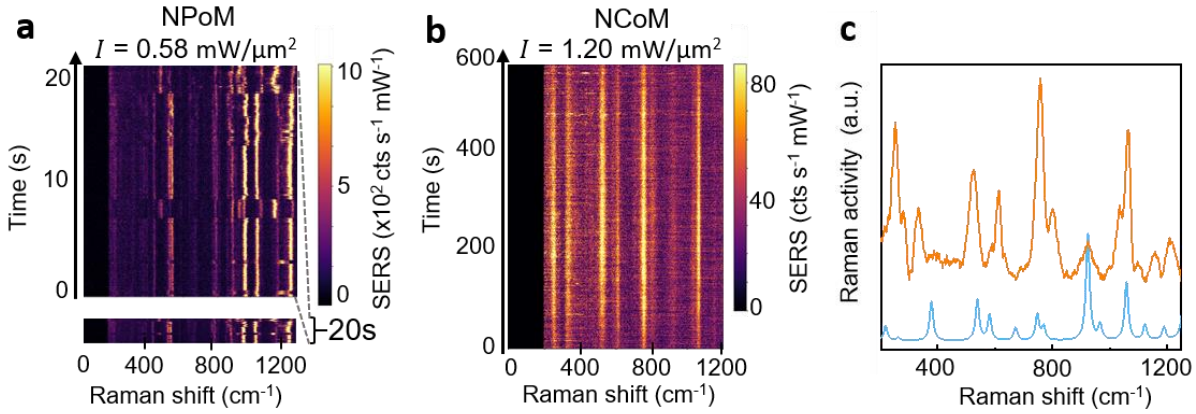

Fig. 5: Facet stability effects on vibrational spectroscopy of molecular monolayers. a) SERS time scan over 20 s for NPoM showing creation of new and previously-dark vibrational modes due to multiple picocavity events. **b)** SERS time scan over 600 s for NCoM revealing high stability of nanocavity modes. **c)** Averaged SERS for NCoM constructs (orange) and calculated DFT (blue) spectra for MPA attached to Au surface and a monodendate O-Au bond with nanoconstruct facet.

The typical solution to low Raman cross-sections is to increase the laser power, however as demonstrated above this leads to unstable enhancements for NPoMs. To evidence this, we use 3-

mercaptopropionic acid (MPA), a molecular spacer which forms gaps of 0.8 nm (see S2 section, SI) with relatively low Raman cross-section (DFT calculations indicate 5-10-fold smaller Raman activity than BPT, Fig. S5 in the SI). When MPA monolayers in NPoM constructs are measured, instead of consistent vibrational lines, sharp distinct peaks are seen which jump around in distinct steps (Fig. 5a). This arises directly from influence of the atom mobility noted above, since 'picocavities'[14] can form in such nanogaps. Adatoms are pulled out from the crystal facet by light and interact with nearby molecules resulting in modified vibrational states and turning on Raman-forbidden transitions. Extremely high SERS intensities from individual perturbed molecules are due to these optical field hot-spots in the 1 nm^3 around each adatom.[14] Since hopping of atoms is rapid on the surface of globular NPs, picocavity events last only a few seconds at room temperature.[47] Consequently, the picocavity occurrence rate can be directly associated with the presence and movement of adatoms in self-assembled nanogaps. Over 20 s measurement at laser intensities of 0.58 $mW/\mu m^2$, many different picocavities are observed in NPoMs, tracking the continuous diffusion of adatoms on the crystal facet (Fig. 5a).

This is compared to recordings of consecutive SERS spectra for NCoMs (Fig. 5b), which despite being at even higher laser intensities of 1.20 $mW/\mu m^2$, show stable nanocavity vibrational modes without forming picocavities.[47] This indicates that fewer adatoms or atomic scale defects are present on the NCoM Au facets. Although both systems give similar (and weak) SERS intensities from the MPA monolayer, for the unstable NPoM system these consistent molecular signatures are drowned out by the much larger picocavity SERS emission strengths.

Even more importantly, the NCoM system is also stable to charge movement within the molecular sandwich. The jumps in the NPoM MPA spectra observed in Fig. 5a arise from a single molecule as indicated by sudden shifts of the entire vibrational line.[14] These signals correspond to the formation of picocavities. Here we study different bonding configurations of MPA and nanoconstruct facet where the best fitting with experimental data corresponds to monodendate binding of one O-Au (Fig. 5c). Specifically, the 560 cm^{-1} vibrational mode corresponds to an O-Au stretch with carboxylate group wagging. Adatom-free facets combined with the elevated intensity thresholds of NCoM constructs thus enable long-time single-molecule SERS measurements on molecules with low Raman cross-section.
To understand the different stability of the NPoM and NCoM systems, we consider the surface energy and stability of each Au atom in their lattice which depends on their bonding strength with nearest neighbours. For face-centred cubic (FCC) crystal structures of Au, the surface free energies U of the primary crystallographic facets follow the trend $U_{\{111\}} < U_{\{001\}} < U_{\{011\}}$.[48]

One factor in the higher stability of NCoMs compared to NPoMs is based on their different crystal habits at the facets of the plasmonic constructs (Fig. 1). Nanocubes have atomically flat {100} facets at their base bounded by thin truncating {110} facets.[49] By contrast globular NPs are composed of many small facets with multiple edges and atomic steps, and typically rest on {111} facets, as observed previously from SEMs of the top facet on the NPoM constructs.[19] Au atoms located close to edges, apexes and steps typically experience lower energy barriers resulting in easier atom mobilisation. Recent findings report that hopping is enhanced at facet edges compared to their centres,[50] as atoms sitting close to edges have fewer bonds with neighbouring Au atoms that hold them in place. Under intense light illumination, the plasmonic Joule losses in the Au deliver energy to surface atoms (either directly or by non-equilibrium heating) inducing higher mobility of these weaker-bonded facet edge atoms. The activation energy for gold adatom surface diffusion is different depending on the crystallographic facet. For {100} the estimated barrier is 3.58 eV (see S1 section, SI),[18] approximately double that on the {111} facet.

Local heating from the incident laser is balanced by cooling through the nanoparticle facet on the mirror, giving temperature rises that can affect the morphology of the nanostructures and consequently their plasmonic resonances. Simulations of nano-optical absorption and heat flow (see S6 section, SI) show that both NCoMs and NPoMs stay below 352K even at 1 mW/μm^2. Compared to nanoparticles embedded in a dielectric, contact to the high thermal conductivity Au substrate here greatly reduces heating. Indeed one way to consider this movement of adatoms is as a type of surface-melting of the nanoparticle, which occurs at temperatures far below their bulk melting point.

Two observations need to be explained in our data on nanocubes: (A) that despite the >100 bar van-der-Waals attraction to the bottom facet, Au atoms cannot move down to the nanoparticle facet to grow its lateral size (no DF redshifts are seen for NCoMs), and (B) that single adatoms are not moved onto or pulled out from the {100} faces of the NCoMs (no picocavities are seen). Both can be accounted for by the higher adatom energy required on {100} facets, so that even if decaying plasmons give their entire energy to an individual Au atom, it is not enough to drive it on the facet. The sub-ps-thermal decay times imply that only one plasmon energy (1-2 eV) is available at any time for each Au atom.

There remains an additional puzzle in the dynamics and stability of these adatoms. It is not yet clear whether the adatoms forming picocavities are pulled directly out of the centre of the facets, or migrate onto the facet from the facet edges. Picocavities in these nanogaps can be formed from adatoms on either facet, the top nanoparticle or the bottom mirror.[47] It is thus surprising (but consistent with other observations) that changing the crystal plane on only the nanoparticle from {111} to {100} can prevent also adatoms on the bottom mirror.[47] Three interpretations are suggested, all of which imply coupling of metal atoms on the top and bottom facets. The first is that adatoms arise from the edges of facets, but can only enter the nanogap cooperatively from top and bottom facet edges (for instance as adatom pairs). The second is that the immense van der Waals forces between the metal faces, together with the strong intermolecular forces in these SAMs, can imprint the {100} facet of the NC onto the mirror underneath, inducing it to reconstruct into the stable {100} form. Finally, it is possible that an element of self-assembly recognition operates, so that NCs approaching the surface seek out grains of the SAM-coated lower mirror that have {100} packing because the molecule order on the top face, or registration of the atoms, provides a stronger attraction. All these remain tentative but intriguing ideas, since such forces would be expected to be very short range.

CONCLUSIONS

In conclusion, we demonstrate nano-construct geometries that can reduce atom hopping/migration events on gold facets. These are problematic in plasmon-based spectroscopies as they lead to transient vibrational states and drifting of plasmon modes in the extreme optical confinement within nanogaps. Two important features distinguish this work from previous work on nanocubes: their stabilisation is by labile citrate ions which are rapidly displaced by the molecular monolayer to give ultrasmall nanogaps, and they are optically accessed from high incident angles to the mirror surface coupling strongly to the (10) mode instead of the weak highly-red-shifted (11) mode.[22]

Intense laser illumination activates hopping of atoms that reconstruct the facet of typical globular NPs and creates atomic scale defects, which shift the local metal permittivity and consequently their plasma frequency.[44] By contrast, NCoMs have elevated energy activation barriers for atoms to mobilise, and thus show significant resilience to constant laser intensity. Atomic scale reconstruction at high power slightly increases the facet widths, observed as redshifts of the spectral position of the plasmon resonances. For NPoMs, these show >25 nm red-shift while for NCoMs these are spectrally stable below 0.2 mW/μm^2. We perform consecutive SERS spectra for NPoM and NCoM geometries to study the dynamics of atom hopping on vibrational spectroscopy of molecular monolayers in nanogaps. For NPoMs, unstable peaks are correlated with the presence of adatoms in the gap, which

are eliminated in NCoMs. We show that molecules with low Raman cross-section self-assembled in nanocavities can be successfully characterised with SERS.

Further investigations using a systematic study of a wide array of NP morphologies will give much information about various atomic and molecular processes at this deeply sub-nm scale. At the same time, the knowledge should be effective in providing much more robust nanocavities for a wide variety of experiments in surface science, photocatalysis and molecular electronics.[51-54]

METHODS

Sample preparation. To prepare atomically smooth Au substrates, we follow the recipe suggested previously.[23] To do so, we used polished 4-inch Si wafers where their surface cleaned thoroughly by ethanol and isopropanol solutions. 100 nm Au deposited directly on a clean Si wafer using a deposition rate of 1 Å/s (LEV Lesker, e-beam evaporator). Further, we glued rectangular pieces of Si (1x1 cm) onto the 100nm Au film using Epo-Tek 377 epoxy and the wafer placed on hotplate at a temperature of 150 °C. Here, we kept the temperature at 150°C for about 2 h and then gradually decrease the temperature in steps of 20 °C (each step 1 h) to avoid thermal stresses. After, the wafer cooled down (overnight) and then the Si pieces pulled off to expose an atomically smooth 100 nm thick Au mirror. For the realisation of single atomic monolayers (SAMs), the Au-coated Si pieces dipped in 1 mM solution of biphenyl-4-thiol (BPT, Sigma Aldrich, 97%) in anhydrous ethanol (Sigma Aldrich, <0.003% H_2O) for 12 h. To form nanometre-scale cavities, 75 nm cubic nanoparticles (NPs) (Nanopartz) and 80 nm globular NPs (BBI Solutions) deposited directly onto the BPT treated Au surface. The deposition time (may vary for NPs batches) is 15 s. TEM images were taken at 200 kV, using an FEI Technai G2 F20 X-TWIN TEM. The cubes, and globular NPs, were drop-casted on carbon-film coated TEM grids.

Experimental setup. All dark-field and SERS spectra measured in a microscope-based setup similar to one reported previously.[24] Briefly, the sample placed on a motorised stage (Prior Scientific H101) which is fully-automated using an in-house code written in Python. We used an Olympus BX51 microscope with a long working distance ×100 NA 0.8 objective (high NA is essential to excite (10) mode). A spectrally filtered 632.8 nm diode laser (Matchbox, Integrated Optics) with output power of around 70 mW and spectral linewidth of 0.1 pm is used as excitation pump. In SERS experiments, we filter laser light with a pair of notch filters centred at 633 ± 2nm (Thorlabs). Further, inelastically scattered light from the nanoconstructs coupled through a tube lens into an Andor Shamrock i303 spectrograph and a Newton EMCCD. For dark-field measurements, we used a halogen lamp to excite our samples. We note that we leave around 30 min to stabilise the lamp's power before starting measurements. The reflected light collected through the same objective and splitted to an imaging camera (Lumenera Infinity3-1) and a fibre-coupled spectrometer (Ocean Optics QEPRO) for dark-field spectroscopy.

ASSOCIATED CONTENT

Supporting information

The Supporting Information is available free of charge on the ACS Publications website at DOI:
Calculations on surface energies of crystal habits, DFT molecular calculations, FDTD near-field simulations, information regarding large area dark field analysis and optical heating calculations.

AUTHOR INFORMATION

Corresponding Author:

Angelos Xomalis; Email: ax210@cam.ac.uk, Jeremy J. Baumberg; Email: jjb12@cam.ac.uk

Author Contributions

A.X. and R.C. performed dark-field and SERS experiments. E.O. and I.S. developed nanocube samples and assist with optical measurements. A.X. and J.H. obtained vibrational spectroscopy and DFT

calculations of MPA self-assembled nanoconstructs. A.X. and R.C. performed optical heating and FDTD near-field simulations. E.C.G., A.F.K. and J.J.B. supervised the research. A.X. and J.J.B. wrote the manuscript. All authors discussed the results and contributed to the final paper.

[†] A.X. and R.C. contributed equally.

The authors declare no competing financial interest.

ACKNOWLEDGMENTS
We acknowledge support from European Research Council (ERC) under Horizon 2020 research and innovation programme THOR (Grant Agreement No. 829067) and POSEIDON (Grant Agreement No. 861950). We acknowledge funding from the EPSRC (Cambridge NanoDTC EP/L015978/1, EP/L027151/1, EP/S022953/1, EP/P029426/1, and EP/R020965/1). R.C. acknowledges support from Trinity College, University of Cambridge.

REFERENCES
1. Anker, J. N.; Hall, W. P.; Lyandres, O.; Shah, N. C.; Zhao, J.; Van Duyne, R. P., Biosensing with Plasmonic Nanosensors. *Nat. Materials* **2008,** *7*, 442–453.
2. Zijlstra, P.; Paulo, P. M.; Orrit, M., Optical Detection of Single Non-Absorbing Molecules Using the Surface Plasmon Resonance of a Gold Nanorod. *Nat. Nanotechnol.* **2012,** *7*, 379-382.
3. Nie, S.; Emory, S. R., Probing Single Molecules and Single Nanoparticles by Surface-Enhanced Raman Scattering. *Science* **1997,** *275*, 1102-1106.
4. Barbry, M.; Koval, P.; Marchesin, F.; Esteban, R.; Borisov, A. G.; Aizpurua, J.; Sánchez-Portal, D., Atomistic Near-Field Nanoplasmonics: Reaching Atomic-Scale Resolution in Nanooptics. *Nano Lett.* **2015,** *15*, 3410-3419.
5. Zhang, R.; Zhang, Y.; Dong, Z.; Jiang, S.; Zhang, C.; Chen, L.; Zhang, L.; Liao, Y.; Aizpurua, J.; Luo, Y. e., Chemical Mapping of a Single Molecule by Plasmon-Enhanced Raman Scattering. *Nature* **2013,** *498*, 82-86.
6. Wang, H.; Brandl, D. W.; Nordlander, P.; Halas, N. J., Plasmonic Nanostructures: Artificial Molecules. *Acc. Chem. Res.* **2007,** *40*, 53-62.
7. Nehl, C. L.; Hafner, J. H., Shape-Dependent Plasmon Resonances of Gold Nanoparticles. *J. Mater. Chem.* **2008,** *18*, 2415-2419.
8. Su, K.-H.; Wei, Q.-H.; Zhang, X.; Mock, J.; Smith, D. R.; Schultz, S., Interparticle Coupling Effects on Plasmon Resonances of Nanogold Particles. *Nano Lett.* **2003,** *3*, 1087-1090.
9. Ciracì, C.; Hill, R.; Mock, J.; Urzhumov, Y.; Fernández-Domínguez, A.; Maier, S.; Pendry, J.; Chilkoti, A.; Smith, D., Probing the Ultimate Limits of Plasmonic Enhancement. *Science* **2012,** *337*, 1072-1074.
10. Baffou, G.; Quidant, R., Thermo-Plasmonics: Using Metallic Nanostructures As Nano-Sources of Heat. *Laser Photonics Rev.* **2013,** *7*, 171-187.
11. Stewart, J. W.; Vella, J. H.; Li, W.; Fan, S.; Mikkelsen, M. H., Ultrafast Pyroelectric Photodetection with On-Chip Spectral Filters. *Nat. Materials* **2020,** *19*, 158-162.
12. Atwater, H. A.; Polman, A., Plasmonics for Improved Photovoltaic Devices. *Nat. Materials* **2010,** *9*, 205-213.
13. Linic, S.; Christopher, P.; Ingram, D. B., Plasmonic-Metal Nanostructures for Efficient Conversion of Solar to Chemical Energy. *Nat. Materials* **2011,** *10*, 911-921.
14. Benz, F.; Schmidt, M. K.; Dreismann, A.; Chikkaraddy, R.; Zhang, Y.; Demetriadou, A.; Carnegie, C.; Ohadi, H.; De Nijs, B.; Esteban, R., Single-Molecule Optomechanics in "Picocavities". *Science* **2016,** *354*, 726-729.
15. Ye, X.; Jin, L.; Caglayan, H.; Chen, J.; Xing, G.; Zheng, C.; Doan-Nguyen, V.; Kang, Y.; Engheta, N.; Kagan, C. R., Improved Size-Tunable Synthesis of Monodisperse Gold Nanorods Through the Use of Aromatic Additives. *ACS Nano* **2012,** *6*, 2804-2817.

16. Chen, H.; Shao, L.; Li, Q.; Wang, J., Gold Nanorods and Their Plasmonic Properties. *Chem. Soc. Rev.* **2013,** *42*, 2679-2724.
17. Zhou, Z.-Y.; Tian, N.; Li, J.-T.; Broadwell, I.; Sun, S.-G., Nanomaterials of High Surface Energy with Exceptional Properties in Catalysis and Energy Storage. *Chem. Soc. Rev.* **2011,** *40*, 4167-4185.
18. Vitos, L.; Ruban, A.; Skriver, H. L.; Kollar, J., The Surface Energy of Metals. *Surf. Sci.* **1998,** *411*, 186-202.
19. Kleemann, M.-E.; Mertens, J.; Zheng, X.; Cormier, S.; Turek, V.; Benz, F.; Chikkaraddy, R.; Deacon, W.; Lombardi, A.; Moshchalkov, V. V., Revealing Nanostructures Through Plasmon Polarimetry. *ACS Nano* **2017,** *11*, 850-855.
20. Benz, F.; Tserkezis, C.; Herrmann, L. O.; De Nijs, B.; Sanders, A.; Sigle, D. O.; Pukenas, L.; Evans, S. D.; Aizpurua, J.; Baumberg, J. J., Nanooptics of Molecular-Shunted Plasmonic Nanojunctions. *Nano Lett.* **2015,** *15*, 669-674.
21. Personick, M. L.; Mirkin, C. A., Making Sense of the Mayhem Behind Shape Control in the Synthesis of Gold Nanoparticles. *J. Am. Chem. Soc.* **2013,** *135*, 18238-18247.
22. Chikkaraddy, R.; Zheng, X.; Benz, F.; Brooks, L. J.; De Nijs, B.; Carnegie, C.; Kleemann, M.-E.; Mertens, J.; Bowman, R. W.; Vandenbosch, G. A., How Ultranarrow Gap Symmetries Control Plasmonic Nanocavity Modes: from Cubes to Spheres in the Nanoparticle-On-Mirror. *ACS Photonics* **2017,** *4*, 469-475.
23. Hegner, M.; Wagner, P.; Semenza, G., Ultralarge Atomically Flat Template-Stripped Au Surfaces for Scanning Probe Microscopy. *Surf. Sci.* **1993,** *291*, 39-46.
24. Benz, F.; Chikkaraddy, R.; Salmon, A.; Ohadi, H.; De Nijs, B.; Mertens, J.; Carnegie, C.; Bowman, R. W.; Baumberg, J. J., SERS of Individual Nanoparticles on a Mirror: Size Does Matter, But So Does Shape. *J. Phys. Chem. Lett* **2016,** *7*, 2264-2269.
25. Gao, B.; Arya, G.; Tao, A. R., Self-Orienting Nanocubes for the Assembly of Plasmonic Nanojunctions. *Nat. Nanotechnol.* **2012,** *7*, 433-437.
26. Bowen, P. T.; Smith, D. R., Coupled-Mode Theory for Film-Coupled Plasmonic Nanocubes. *Phys. Rev. B* **2014,** *90*, 195402.
27. Lin, Q.-Y.; Li, Z.; Brown, K. A.; O'Brien, M. N.; Ross, M. B.; Zhou, Y.; Butun, S.; Chen, P.-C.; Schatz, G. C.; Dravid, V. P., Strong Coupling Between Plasmonic Gap Modes and Photonic Lattice Modes in DNA-Assembled Gold Nanocube Arrays. *Nano Lett.* **2015,** *15*, 4699-4703.
28. Hoang, T. B.; Akselrod, G. M.; Mikkelsen, M. H., Ultrafast Room-Temperature Single Photon Emission from Quantum Dots Coupled to Plasmonic Nanocavities. *Nano Lett.* **2016,** *16*, 270-275.
29. Akselrod, G. M.; Weidman, M. C.; Li, Y.; Argyropoulos, C.; Tisdale, W. A.; Mikkelsen, M. H., Efficient Nanosecond Photoluminescence from Infrared Pbs Quantum Dots Coupled to Plasmonic Nanoantennas. *ACS Photonics* **2016,** *3*, 1741-1746.
30. Lee, S. Y.; Hung, L.; Lang, G. S.; Cornett, J. E.; Mayergoyz, I. D.; Rabin, O., Dispersion in the SERS Enhancement with Silver Nanocube Dimers. *ACS Nano* **2010,** *4*, 5763-5772.
31. Grillet, N.; Manchon, D.; Bertorelle, F.; Bonnet, C.; Broyer, M.; Cottancin, E.; Lermé, J.; Hillenkamp, M.; Pellarin, M., Plasmon Coupling in Silver Nanocube Dimers: Resonance Splitting Induced by Edge Rounding. *ACS Nano* **2011,** *5*, 9450-9462.
32. Luo, Y.; Shepard, G. D.; Ardelean, J. V.; Rhodes, D. A.; Kim, B.; Barmak, K.; Hone, J. C.; Strauf, S., Deterministic Coupling of Site-Controlled Quantum Emitters in Monolayer WSe_2 to Plasmonic Nanocavities. *Nat. Nanotechnol.* **2018,** *13*, 1137-1142.
33. Sun, J.; Hu, H.; Zheng, D.; Zhang, D.; Deng, Q.; Zhang, S.; Xu, H., Light-Emitting Plexciton: Exploiting Plasmon–Exciton Interaction in the Intermediate Coupling Regime. *ACS Nano* **2018,** *12*, 10393-10402.
34. Han, X.; Wang, K.; Xing, X.; Wang, M.; Lu, P., Rabi Splitting in a Plasmonic Nanocavity Coupled to a WS_2 Monolayer at Room Temperature. *ACS Photonics* **2018,** *5*, 3970-3976.
35. Robatjazi, H.; Lou, M.; Clark, B. D.; Jacobson, C. R.; Swearer, D. F.; Nordlander, P.; Halas, N. J., Site-Selective Nanoreactor Deposition on Photocatalytic Al Nanocubes. *Nano Lett.* **2020,** *20*, 4550−4557.
36. Clark, B. D.; Jacobson, C. R.; Lou, M.; Renard, D.; Wu, G.; Bursi, L.; Ali, A. S.; Swearer, D. F.; Tsai, A.-L.; Nordlander, P., Aluminum Nanocubes Have Sharp Corners. *ACS Nano* **2019,** *13*, 9682-9691.

37. Wang, X.; Ma, G.; Li, A.; Yu, J.; Yang, Z.; Lin, J.; Li, A.; Han, X.; Guo, L., Composition-Adjustable Ag–Au Substitutional Alloy Microcages Enabling Tunable Plasmon Resonance for Ultrasensitive SERS. *Chem. Sci.* **2018,** *9*, 4009-4015.
38. Kongsuwan, N.; Demetriadou, A.; Horton, M.; Chikkaraddy, R.; Baumberg, J. J.; Hess, O., Plasmonic Nanocavity Modes: from Near-Field to Far-Field Radiation. *ACS Photonics* **2019,** *7*, 463–471.
39. Baumberg, J. J.; Aizpurua, J.; Mikkelsen, M. H.; Smith, D. R., Extreme Nanophotonics from Ultrathin Metallic Gaps. *Nat. Materials* **2019,** *18*, 668-678.
40. Mertens, J.; Demetriadou, A.; Bowman, R.; Benz, F.; Kleemann, M.-E.; Tserkezis, C.; Shi, Y.; Yang, H.; Hess, O.; Aizpurua, J., Tracking Optical Welding through Groove Modes in Plasmonic Nanocavities. *Nano Lett.* **2016,** *16*, 5605-5611.
41. Kleemann, M.-E.; Chikkaraddy, R.; Alexeev, E. M.; Kos, D.; Carnegie, C.; Deacon, W.; De Pury, A. C.; Große, C.; De Nijs, B.; Mertens, J., Strong-Coupling of WSe_2 in Ultra-Compact Plasmonic Nanocavities at Room Temperature. *Nat. Commun.* **2017,** *8*, 1-7.
42. Sigle, D. O.; Mertens, J.; Herrmann, L. O.; Bowman, R. W.; Ithurria, S.; Dubertret, B.; Shi, Y.; Yang, H. Y.; Tserkezis, C.; Aizpurua, J., Monitoring Morphological Changes in 2D Monolayer Semiconductors Using Atom-Thick Plasmonic Nanocavities. *ACS Nano* **2015,** *9*, 825-830.
43. Lin, K.-Q.; Yi, J.; Zhong, J.-H.; Hu, S.; Liu, B.-J.; Liu, J.-Y.; Zong, C.; Lei, Z.-C.; Wang, X.; Aizpurua, J., Plasmonic Photoluminescence for Recovering Native Chemical Information from Surface-Enhanced Raman Scattering. *Nat. Commun.* **2017,** *8*, 1-9.
44. Carnegie, C.; Urbieta, M.; Chikkaraddy, R.; de Nijs, B.; Griffiths, J.; Deacon, W. M.; Kamp, M.; Zabala, N.; Aizpurua, J.; Baumberg, J. J., Flickering Nanometre-Scale Disorder in a Crystal Lattice Tracked By Plasmonic Flare Light Emission. *Nat. Commun.* **2020,** *11*, 1-9.
45. Hugall, J. T.; Baumberg, J. J., Demonstrating Photoluminescence from Au is Electronic Inelastic Light Scattering of a Plasmonic Metal: The Origin Of SERS Backgrounds. *Nano Lett.* **2015,** *15*, 2600-2604.
46. Tserkezis, C.; Esteban, R.; Sigle, D. O.; Mertens, J.; Herrmann, L. O.; Baumberg, J. J.; Aizpurua, J., Hybridization of Plasmonic Antenna and Cavity Modes: Extreme Optics of Nanoparticle-On-Mirror Nanogaps. *Phys. Rev. A* **2015,** *92*, 053811.
47. Carnegie, C.; Griffiths, J.; de Nijs, B.; Readman, C.; Chikkaraddy, R.; Deacon, W. M.; Zhang, Y.; Szabó, I. n.; Rosta, E.; Aizpurua, J., Room-Temperature Optical Picocavities Below $1nm^3$ Accessing Single-Atom Geometries. *J. Phys. Chem. Lett* **2018,** *9*, 7146-7151.
48. Galanakis, I.; Papanikolaou, N.; Dederichs, P., Applicability of the Broken-Bond Rule to the Surface Energy of the FCC Metals. *Surf. Sci.* **2002,** *511*, 1-12.
49. Sun, Y.; Xia, Y., Shape-Controlled Synthesis of Gold and Silver Nanoparticles. *Science* **2002,** *298*, 2176-2179.
50. Katz-Boon, H.; Walsh, M.; Dwyer, C.; Mulvaney, P.; Funston, A. M.; Etheridge, J., Stability of Crystal Facets in Gold Nanorods. *Nano Lett.* **2015,** *15*, 1635-1641.
51. Kale, M. J.; Avanesian, T.; Christopher, P., Direct Photocatalysis by Plasmonic Nanostructures. *ACS Catalysis* **2014,** *4*, 116-128.
52. Zhang, X.; Chen, Y. L.; Liu, R.-S.; Tsai, D. P., Plasmonic Photocatalysis. *Rep. Prog. Phys.* **2013,** *76*, 046401.
53. Lacroix, J. C.; Van Nguyen, Q.; Ai, Y.; Van Nguyen, Q.; Martin, P.; Lacaze, P. C., From Active Plasmonic Devices to Plasmonic Molecular Electronics. *Polym. Int.* **2019,** *68*, 607-619.
54. Wang, T.; Nijhuis, C. A., Molecular Electronic Plasmonics. *Appl. Mater. Today* **2016,** *3*, 73-86.